PHYSICAL REVIEW B **83**, 075409 (2011)

Morphological instability of the Cu(110)–(2 × 1)–O surface under thermal annealing

Laurent Guillemot and Kirill Bobrov
Institut des Sciences Moléculaires d'Orsay, Centre National de la Recherche Scientifique (CNRS),
Université Paris-Sud 11, F-91405 Orsay, France

(Received 12 May 2010; revised manuscript received 27 August 2010; published 8 February 2011)

We present a scanning tunneling microscope study on reactivity of chemisorbed oxygen on the Cu(110)–(2 × 1)–O surface. We have found that the Cu(110)–(2 × 1)–O surface is intrinsically unstable under thermal annealing in the 400–900 K range. In the 455–570 K range, the surface undergoes faceting. The orientational transition of the adsorbed oxygen phase displays wide [110] terraces, covered by (2 × 1)–O bands self-assembled into a superstructure, as well as bunches of oxygen-free narrow terraces. We found that the wide [110] terraces are intrinsically unstable against further restructuring at their edges. The restructuration is driven by reversible thermal dissociation of the (2 × 1)–O bands. The slightly uneven oxygen band density between terraces, consequently differing in reactivity with respect to Cu–O fragments, induces Cu atom transport between their edges. The interplay between thermal dissociation of the (2 × 1)–O bands and long-range elastic relaxation of the strained surface is suggested to be the origin of the observed inhomogeneous oxygen distribution. In the 570–810 K range the Cu atom transport reveals continuous growth of the oxygenated [110] terraces. We discuss in detail the mechanism of the Cu transport, which results in a rapid propagation of the oxygenated terraces as well as a strain development on the surface.

DOI: 10.1103/PhysRevB.83.075409 PACS number(s): 68.03.Cd, 68.37.Ef, 68.65.Cd, 68.43.Jk

I. INTRODUCTION

The oxygen-induced restructuring of the Cu(110) surface has attracted much interest for the past two decades.[1–13] Molecular oxygen adsorbs dissociatively on the Cu(110) surface at room temperature (RT), inducing (2 × 1) "added-row" reconstruction.[1] Coulman *et al*. have demonstrated[1] that the reconstruction is rather different from a solid-solid transformation and can be considered as a "true" reconstruction proceeding via precipitation of a solid from a fluid mixed phase. The chemisorbed oxygen traps Cu adatoms, evaporated mostly from terrace edges, into a two-dimensional (2D) fluid phase. The precipitation occurs from the fluid phase consisting of the Cu–O precursors thermally diffusing across the surface. Short-range attractive Cu–O interaction causes solid nuclei to precipitate into (2 × 1)–reconstructed Cu–O chains (added rows) on top of surface terraces.

The reconstruction reveals an anisotropically strained Cu(110)–(2 × 1)–O surface owing to the stress difference between the areas covered by the Cu–O chains and the bare surface.[2–4] At submonolayer coverage long-range elastic relaxation of the strained surface induces spatial separation of the Cu–O chains into distinct bands extending on the whole terrace width along the [001] direction.[2] The separation is kinetically hindered at RT.[2] However, a mild thermal annealing at 640 K enhances greatly the adatom mobility enough to reach the relaxation and form an ordered 2D domain pattern consisting of alternating (2 × 1)–O bands and bare surface strips.[2] Nowadays the Cu(110)–(2 × 1)–O domain pattern is considered as a promising nanoscale template for usage in molecular electronics.[14,15]

Since Kern's discovery[2] of the domain pattern formation in 1991, it has been tentatively assumed that the oxygen-induced restructuring of the Cu(110) surface is limited to the reconstruction and relaxation processes. Here we report on a phenomenon, namely, the morphological instability of the Cu(110)–(2 × 1)–O surface under thermal annealing. We will show that the interplay between the short-range and long-range interactions on the strained surface makes the surface thermodynamically unstable against further restructuring.

II. EXPERIMENTAL

A single-crystal Cu(110) sample cut with a maximal achievable accuracy of ~0.1° was used in this study. The thoroughly polished Cu(110) sample was cleaned *in situ* by repeated cycles of sputtering by 1-keV Ar^+ ions at grazing incident angles, followed by thermal annealing at 930 K. Oxygen adsorption on the clean Cu(110) surface was done at RT by exposing the surface to molecular oxygen at $P = 2$–8×10^{-10} mbar for adsorption doses in the 0.1–4 Langmuir (L) range, with simultaneous recording of STM topographies. The oxygen coverage at each adsorption dose was determined by counting the (2 × 1)–O rows on the corresponding STM topographies. The cleanliness of the oxygen-covered surface was controlled by Auger electron spectroscopy (AES) and STM, and no impurities were detected. Thermal treatment of the oxygenated surface consisted of annealing and cooling down cycles at progressively increasing temperatures in the 390–900 K range. Each annealing was performed by keeping the upper temperature constant for 10 min. STM topographies were recorded at RT in a constant current mode by tunneling from occupied surface states. Typical tunneling conditions were as follows: $U_{\text{bias}} = -1.5$ V, $I_t = 0.5$ nA. The surface was scanned a a sufficiently long time until "trapping" of an O atom by the STM tip, typically occurring on Cu(110)–(2 × 1)–O surfaces,[6,7] was detected. Height profiles, taken on the (2 × 1)–O phase, confirmed the O-type character of the STM tip. Topography distortion was then corrected using the known geometry of the Cu(110)–(2 × 1)–O adsorption phase as a reference.

III. RESULTS AND DISCUSSION

A. Oxygen adsorption on the Cu(110) surface: Stabilization effect

Figure 1 visualizes the evolution of the clean Cu(110) surface under oxygen adsorption. Oxygen adsorption in the 0.18–0.45 L range resulted in the formation of the Cu–O chains assembled into the (2×1)–O bands on the $T_1 - T_4$ terraces. The bands are visible on the STM topographies as dark or bright lines running in the [001] direction. The temporary switching of the topography contrast reflects changes in the tunneling junction when the STM tip spontaneously captures or drops oxygen from its apex[6,7] during the ongoing adsorption. Once nucleated, the Cu–O chains propagate rapidly over surface terraces by incorporation of Cu–O fragments precipitated from the Cu–O fluid phase.[1,8,9]

In this part of the study we focus on the role of the (2×1)–O bands in the stabilization of terrace edges against Cu abstraction. The abstraction process has been studied previously under oxygen adsorption.[8–10] It was found that the Cu–O chains served as a barrier for Cu atoms diffusion in the $[1\bar{1}0]$ direction that produced characteristic kinked structures at the terrace edges.[8] It was suggested that the Cu abstraction rate might depend on the particular location on the terrace edge.[9] In this study we evaluate quantitatively these effects.

Figure 1(a) shows that the produced (2×1)–O bands represent an obstacle to the Cu abstraction. The abstraction process proceeds mainly in the $[1\bar{1}0]$ direction and is hampered when the etching front on a particular terrace edge encounters (2×1)–O bands already nucleated above. As a result, characteristic "kinks" develop (line C in Fig. 1) and the terrace edges become decorated by the (2×1)–O bands. Evolution of the terrace edge morphology with the oxygen exposure [Figs. 1(b)–1(d)] indicates anisotropy of the Cu abstraction and stabilization of the terrace edges by the (2×1)–O bands. Evolution of a specific location [marked by an arrow in Fig. 1(a)] illustrates well the former phenomenon. The small increase in the oxygen coverage induces rapid removal of Cu atoms in the $[1\bar{1}0]$ direction, revealing a narrow lacuna labeled as B in Fig. 1(b). The stabilization effect can be first deduced considering the lacuna expansion. The A and B lacunas [Figs. 1(b) and 1(c)], having few (2×1)–O bands on their edges, expand rapidly in the [001] direction. By contrast, the T_3 terrace edge (line C), having a sufficiently high density of the (2×1)–O bands, remains almost intact under the oxygen attack [Figs. 1(a)–1(d)]. However, the stabilization effect does not provide full protection of the terrace edges—it only hampers Cu removal. Etching is continued in the [001] direction, as can be seen in Fig. 1(d). It leaves narrow "teeth" (2.0 ± 0.2 nm width, white arrow) and wider lacunas (at least 5.4 nm wide, black arrow) on the terrace edges. Formation of the narrow teeth manifests the stabilization effect. Chemisorbed oxygen attacks first the edges that are less oxygen bordered. It etches out the Cu substrate in between the (2×1)–O bands, leaving the (2×1)–O teeth visible from the very beginning of the adsorption process [lacuna A in Fig. 1(a)]. The asymmetry in width of the teeth and lacunas represents the third manifestation of the stabilization effect when a uniform etching of the Cu substrate would reveal teeth and lacunas of near equal width. The distance between the (2×1)–O bands is comparable to their width [Fig. 1(d)], and the lacunas are clearly wider than the teeth [Fig. 1(d)]. It further confirms that the (2×1)–O bands stabilize the terrace edges, preventing formation of narrower lacunas, although their formation would be geometrically possible.

The stabilization effect is overcome at higher oxygen coverage [Fig. 2(a)]. Now mobile oxygen induces unspecific Cu removal from the Cu(110) substrate. Figure 2(a) indicates that lacunas are produced both at terrace edges and in the middle of terraces (dark quasirectangular patches). The width asymmetry detected previously is now absent; the teeth and lacunas of

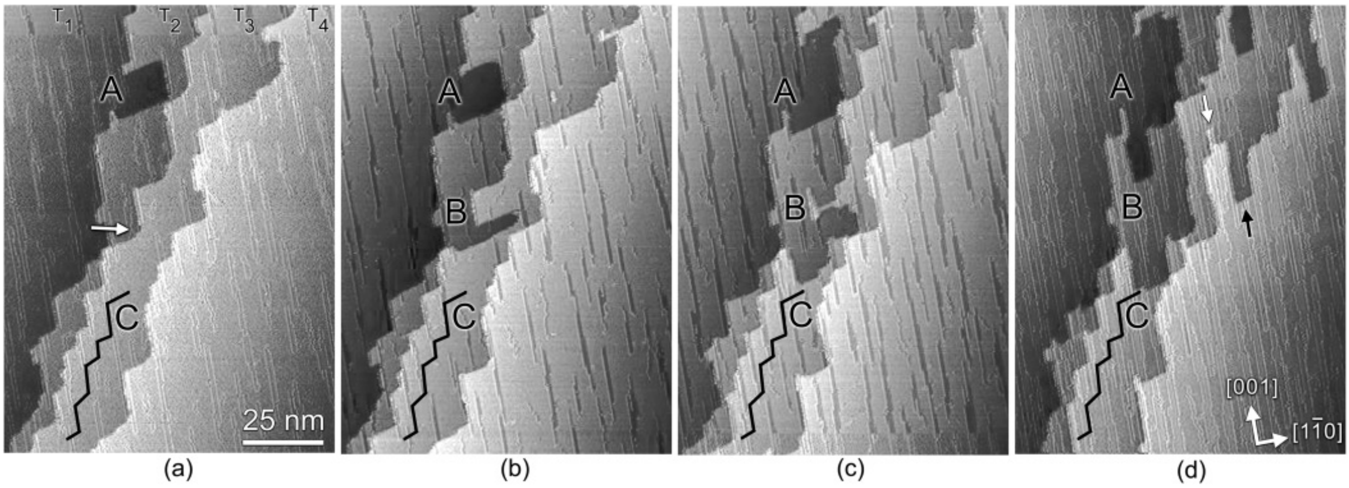

FIG. 1. STM topographies of the Cu(110) surface exposed to oxygen at (a) $D = 0.18$ L ($\theta_O = 0.035$ ML), (b) $D = 0.21$ L ($\theta_O = 0.040$ ML), (c) $D = 0.32$ L ($\theta_O = 0.062$ ML), and (d) $D = 0.45$ L ($\theta_O = 0.086$ ML). Flat monoatomic height terraces are marked as $T_1 - T_4$ in ascending order. The dark and bright lines in the [001] direction represent the (2×1)–O bands developed on the terraces under oxygen adsorption. Lacunas on the T_2 and T_3 terrace edges are marked as A and B, respectively. Line C follows the T_3 terrace edge geometry and serves as a guide to the eye. Both the form and lateral position of line C is identical for all the topographies. The white and black arrows on (d) designate the "teeth" and "lacunas" on the T_4 terrace edges, respectively.

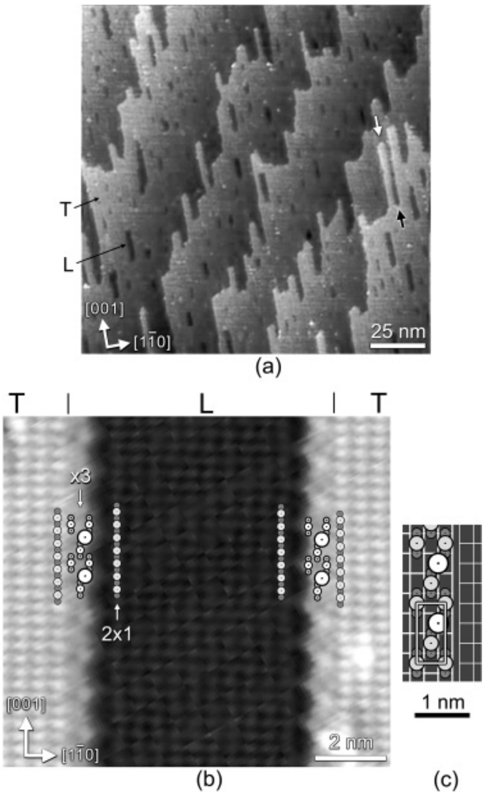

FIG. 2. Oxygen adsorption on the Cu(110) surface at saturation coverage. (a) STM topography of the Cu(110)–(2 × 1)–O surface saturated with oxygen at RT. The arrows mark lacunas (*L*) and terraces (*T*). (b) STM topography of an individual lacuna (*L*) produced on an atomically flat terrace (*T*) of the surface. The bright and dark circles represent Cu and O atoms, respectively, belonging to the ×3 and (2 × 1)–O phases. (c) Structural model of the ×3 phase. The closed-packed rows of the Cu substrate are shown as white lines. The bright and dark circles represent Cu and O atoms assembled into CuO_2 units, and Cu adatoms are shown as white circles. The unit cell is shown by a black and white rectangle.

nearly equal width coexist at the edges. A newly reconstructed linear "×3" phase is produced at the lacuna borders, decorating their [001] steps [Fig. 2(b)]. Its structural model is shown in Fig. 2(c). The ×3 phase ($\theta_O = 12/39$ ML) occupies ~10% of the total surface area that implies $\theta_O \sim 0.48$ ML as saturation coverage.

B. Morphological instability of the Cu(110)–(2 × 1)–O surface: Saturation coverage

A mild thermal annealing of the saturated Cu(110)–(2 × 1)–O surface at 400–460 K (Fig. 3) induces a profound surface rearrangement characterised by (i) refilling of the lacunas visible previously in Fig. 2(a) with Cu atoms and restoration of flat surface terraces, (ii) vanishing of the teeth and lacunas and a general smoothing of the terrace edges, (iii) partial disappearance of the Cu–O chains and consequent reduction of oxygen coverage from ~0.48 ML down to 0.34 ± 0.04 ML, and (iv) segregation of the remaining chains into (2 × 1)–O bands, forming a poorly ordered Cu(110)–(2 × 1)–O domain pattern. The alternating dark and bright strips visible on the STM topography of the domain pattern (Fig. 3) represent the (2 × 1)–O bands and clean surface areas, respectively.

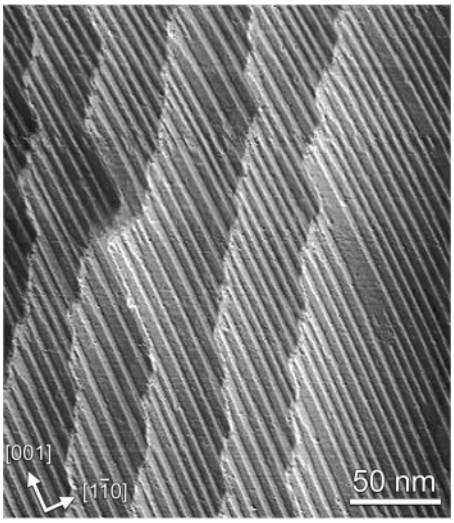

FIG. 3. STM topography of the Cu(110)–(2 × 1)–O surface saturated with oxygen at RT followed by thermal annealing at 400 K for 10 min.

We figure out the mechanism of the surface rearrangement on the basis of the one proposed by Coulman *et al.*[1] for the surface reconstruction. We propose that precipitation of solid nuclei from the Cu–O fluid phase into the Cu–O chains is a reversible process. Then, the fluid phase can be formed on the surface not only by oxygen coming from the gas phase that abstracts Cu atoms, but also by reversible thermal dissociation of the Cu–O chains:

$$[\mathrm{Cu{-}O}]_{(\mathrm{solid})} \xleftrightarrow{t,{}^\circ\mathrm{C}} [\mathrm{Cu{-}O}]_{(\mathrm{fluid})}. \qquad (1)$$

In fact, this thermal dissociation of the Cu–O chains included in the (2 × 1)–O bands can be detected easily at submonolayer coverage even at RT, as shown in Fig. 4(a).

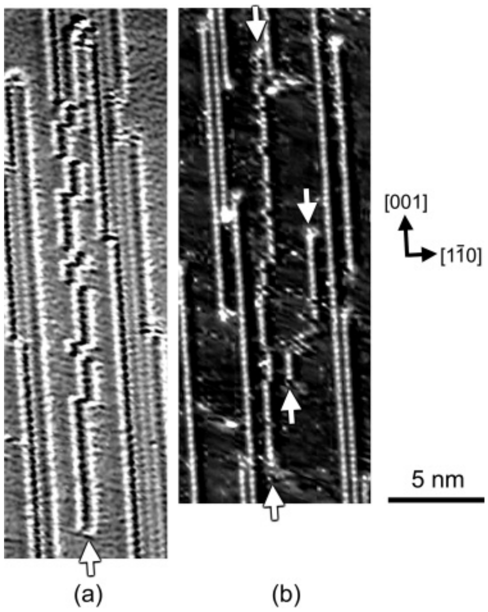

FIG. 4. STM topographies of the Cu(110)–(2 × 1)–O surfaces at (a) 0.20 and (b) 0.14 ML oxygen coverage. Thermally diffusing Cu–O chains are specified by arrows.

Concerted and reversible detachment of two adjacent Cu–O chain fragments from a (2×1)–O band can be seen in Fig. 4(a). One never noticed detachment of the larger chain aggregates at RT. It suggests an increasing thermodynamic stability of the (2×1)–O bands as a function of their width. Once being completely detached, the Cu–O chain fragments diffuse rapidly across the surface. Their thermal diffusion at the very initial stage of oxygen adsorption can be seen in Fig. 4(b). At RT segregation of the Cu–O chains is kinetically hampered. So at low coverage the chains exist mostly in the single or double configuration. Thermal diffusion of the single Cu–O chains is marked by arrows in Fig. 4(b). The apparent “fragmentation” of the straight chains simply means that the Cu–O chains move faster than the scanning STM tip.[9]

While thermal annealing is stopped and the surface is cooling down, the fluid phase can precipitate via two different channels. The Cu–O fragments can either reattach to the portion of still existing (2×1)–O bands [Eq. (1)] or further dissociate by incorporation of Cu atoms into terrace edges, inducing lateral terrace growth:

$$[\mathrm{Cu{-}O}]_{(\mathrm{fluid})} + \mathrm{Cu}_{(\mathrm{solid})} \leftrightarrow [\mathrm{Cu{-}Cu}]_{(\mathrm{solid})} + \mathrm{O}_{(\mathrm{ad})}. \qquad (2)$$

It seems that both events have a comparable probability, as occasional growth of terraces has been observed under oxygen adsorption.[1] In the case of the saturated Cu(110)–(2×1)–O surface, shown in Fig. 2(a), the incorporation is greatly enhanced owing to the energy gained under lacuna refilling because restoration of flat Cu(110) terraces reduces the density of thermodynamically unfavorable surface steps.[16]

The Cu–O fragments precipitate on the lacuna edges, donating their Cu atoms and releasing oxygen adatoms [Eq. (2)]. Therefore, not all the initially existing Cu–O chains are restored under precipitation; some of them have been consumed by the lacuna refilling. That is visible in Fig. 3 by formation of strips of a clean surface, which divide the (2×1)–O phase into distinct domains. The released oxygen adatoms can either reabstract Cu atoms from terrace edges [Eq. (2)] or even recombine on the surface and desorb as a dioxygen molecule:

$$\mathrm{O}_{(\mathrm{ad})} + \mathrm{O}_{(\mathrm{ad})} \rightarrow \mathrm{O}_{2(\mathrm{gas})}. \qquad (3)$$

The former process is strongly hampered in the case of the saturated surface by the high density of the (2×1)–O bands, which protect the terrace edges against oxygen attack (see Sec. III A). The oxygen, therefore, leaves the surface by recombination [Eq. (3)].

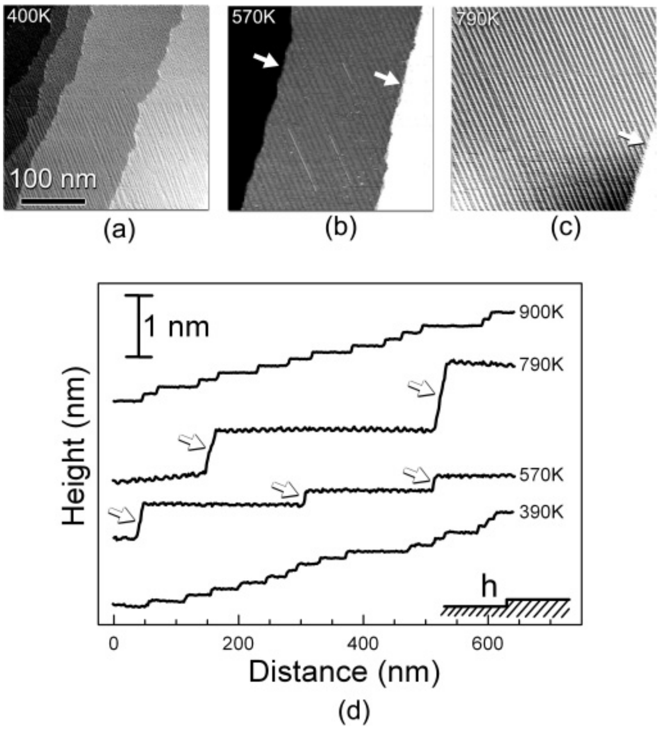

FIG. 5. Thermally induced rearrangement of the Cu(110)–(2×1)–O surface. (a)–(c) STM topographies of the Cu(110)–(2×1)–O surface as a function of thermal annealing. The arrows mark step bunches. (d) STM height profiles taken perpendicular to step bunches (marked by arrows) as a function of the annealing temperature. A monoatomic step (h) is shown schematically.

C. Morphological instability of the Cu(110)–(2 × 1)–O surface: Submonolayer coverage

Surprisingly, the surface rearrangement is not over after the lacuna refilling and restoration of the flat terraces. At higher annealing temperatures the Cu(110)–(2×1)–O surface undergoes a global rearrangement, which is seen clearly in Figs. 5(a)–5(c) by (i) a steep increase in the surface terrace width and (ii) the formation of step bunches of different heights (marked by arrows) separating the wide terraces. The structure of a typical step bunch is shown in Fig. 6(a). All the small terraces of the bunch are separated by monoatomic steps [Fig. 6(b)]. The narrow $T_1 - T_4$ terraces are not covered by (2×1)–O chains (contrary to the T_5 terrace) nor oxygen on their borders; the fuzzy appearance of their step edges is characteristic of a clean surface.[12] A statistical analysis of many step bunches reveals that a typical step bunch includes a bundle of 2–14 clean terraces, 2–10 nm wide, separated by monoatomic steps. All the terraces remain atomically flat during the rearrangement, and we measured on the STM profiles no substantial variation of the sample miscut angle. It means that the substantial Cu transport occurs between the

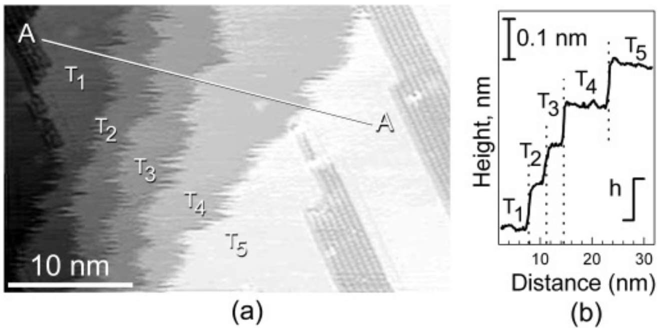

FIG. 6. Structure of a typical step bunch. (a) STM topography of a typical bunch. The white line A marks the lateral position of the STM height profile shown in (b). The surface terraces are marked as $T_1 - T_5$ in ascending order. (b) STM height profile recorded across the step bunch. A monoatomic step (h) is shown for comparison.

terrace edges. Now we consider in detail the thermodynamics of the Cu transport as a function of annealing temperature.

1. Thermally induced surface faceting

A question immediately arising is, to what extent the surface rearrangement can be explained simply by surface faceting,[16] which is known to occur on vicinal Cu surfaces exposed to oxygen.[17] It was shown that oxygen chemisorption on vicinal Cu(11*n*) surfaces induced a so-called orientational separation[16] of the oxygen phase between flat facets, on which the Cu–O chains were nucleated, and monoatomic surface steps, which remained oxygen free under the adsorption.[17] The energy gain, associated with the oxygen-induced reconstruction of the flat facets, made these vicinal surfaces unstable against faceting. Under increasing oxygen coverage, the redistribution of Cu atoms between surface steps favored laterally expanding flat terraces, on which the Cu–O chains increased in density, and oxygen-free monoatomic steps, gradually gathering into bunches.

Jeong and Williams[16] have shown that under thermal equilibrium the orientational phase transition is determined by a balance between the free energy of the clean surface [Eq. (4)] and the oxygenated surface [Eq. (5)],

$$f = f_0 + \beta\rho/h + g\rho^3, \tag{4}$$

where f_0 is the free energy of the [110] plane, f is the free energy of the clean surface having ρ density of wandering surface steps of h height, β is the energy required to create an isolated surface step, and g is the step interaction parameter,

$$f(\theta_O) = [f_0 - \Delta f(\theta_O)] + (\beta + \Delta\beta)p/h + g\rho^3(\theta_O), \tag{5}$$

where $f(\theta_O)$ is the free energy of the oxygenated surface having θ_O oxygen coverage, $\Delta f(\theta_O)$ is the energy gain of the [110] plane reconstruction, $\Delta\beta$ is the oxygen-induced increase in the step free energy, and $\rho(\theta_O)$ is the step density at the bunches.

Therefore, the driving force of the surface faceting comes from the continuous gain of energy owing to the reconstruction as long as it exceeds the energy loss associated with increasing step density in the bunches.

In order to evaluate the role the surface faceting plays in our case (Fig. 5), we analyze in detail the orientation of the step bunches and their morphology as a function of annealing temperature (Fig. 7). The step bunches first appeared on the surface after its thermal annealing at 455 K [Fig. 7(a)]. Below this threshold (zone A), the surface mobility is too low to make the Cu transport efficient. Surface faceting starts at a higher temperature (zone B). Reversible thermal dissociation of the Cu–O chains [Eq. (1)] into the fluid phase triggers the Cu transport between surface terraces, as is shown schematically in Figs. 7(d) and 7(e). The phase transition takes place. The (2 × 1)–O bands leave the step edges and precipitate into an ordered superstructure on the flat terraces [Fig. 7(c)], and the oxygen-free surface steps gather into step bunches [Fig. 7(c)].

It is important to notice that the orientational phase transition is completed at $T = 570$ K, establishing a thermal equilibrium. No further relaxation of the Cu(110)–(2 × 1)–O superstructure was detected at higher temperature. The superstructure produced on the wide terraces after the 810 K annealing (topography C) was almost identical to that produced at 570 K (topography B). In the meantime, the step density remains essentially the same. It even slightly decreases, probably following the slight decrease of oxygen coverage owing to a slight thermal desorption of oxygen. By contrast, the surface rearrangement was not over at 570 K. It even accelerated at higher temperatures, as shown in Fig. 5. The averaged terrace width increases from ∼220 nm up to ∼450 nm in the 570–810 K range [Fig. 7(b)]. The corresponding step bunch height steeply increases, gathering now up to 14 monoatomic surface steps [Fig. 7(c)].

Therefore, surface faceting itself cannot explain the observed rearrangement. According to Eq. (5) there is no further decrease in the surface free energy when both oxygen coverage and step density remain constant. Consequently, there is no driving force left for faceting when thermal equilibrium between the two phases—the Cu(110)–(2 × 1)–O superstructure and the “step bunch” phase—is achieved.

2. The mechanism of the surface rearrangement

The STM topography shown in Fig. 8 represents a key observation, which allowed us to propose a mechanism for the surface rearrangement. This topography, recorded in the surface faceting regime (zone B in Fig. 7), indicates the *inhomogeneous* distribution of the Cu–O chains between different terraces. The T_1 terrace is covered mainly with wide (2 × 1)–O bands, whereas the T_2 and T_3 terraces contain narrower bands, providing a lower band density on the terrace edges.

We propose the following mechanism of the surface rearrangement shown schematically in Fig. 9. As we discussed in Sec. III B, incorporation of the Cu–O fragments in the terrace edges releases oxygen adatoms [Eq. (2)]. The mobile oxygen abstracts preferentially Cu atoms from the edges with lower (2 × 1)–O band density [edge A in Fig. 9; the (2 × 1)–O bands are omitted for simplicity]. The edges retract and the corresponding terraces shrink. On those terraces, where the density of (2 × 1)–O bands happens to be above the stabilization threshold, the Cu incorporation dominates (edge B in Fig. 9). The corresponding edges propagate and the terraces expand laterally.

As we mentioned in Sec. III C 1, the Cu–O fragments precipitate into the (2 × 1)–O chains, lengthening the (2 × 1)–O bands across the expanding terraces [Figs. 7(c) and 7(e)]. We stress that such lengthening of the (2 × 1)–O bands in the [001] direction provides the energetic gain of the rearrangement process. It is well known that growth of the Cu–O chains in the [001] direction on the Cu(110) surface is driven by a strong, attractive interaction between O and Cu adatoms.[1,9,18] Here, the strong, attractive Cu–O interaction manifests itself by reduction of the thermodynamically unfavorable Cu–O chain boundaries during the dissociation and precipitation process, as it is shown schematically in Figs. 7(d) and 7(e).

The rearrangement of the surface terraces visible on the STM topographies [Figs. 8(a) and 8(b)] is fully consistent with the proposed mechanism. Meandering of the T_3 terrace edge modifying the T_3 terrace width (zones B–D) correlates well with the (2 × 1)–O band density. This can be understood either as the T_3 terrace edge retracts, most because of Cu abstraction at the location with the lowest (2 × 1)–O band

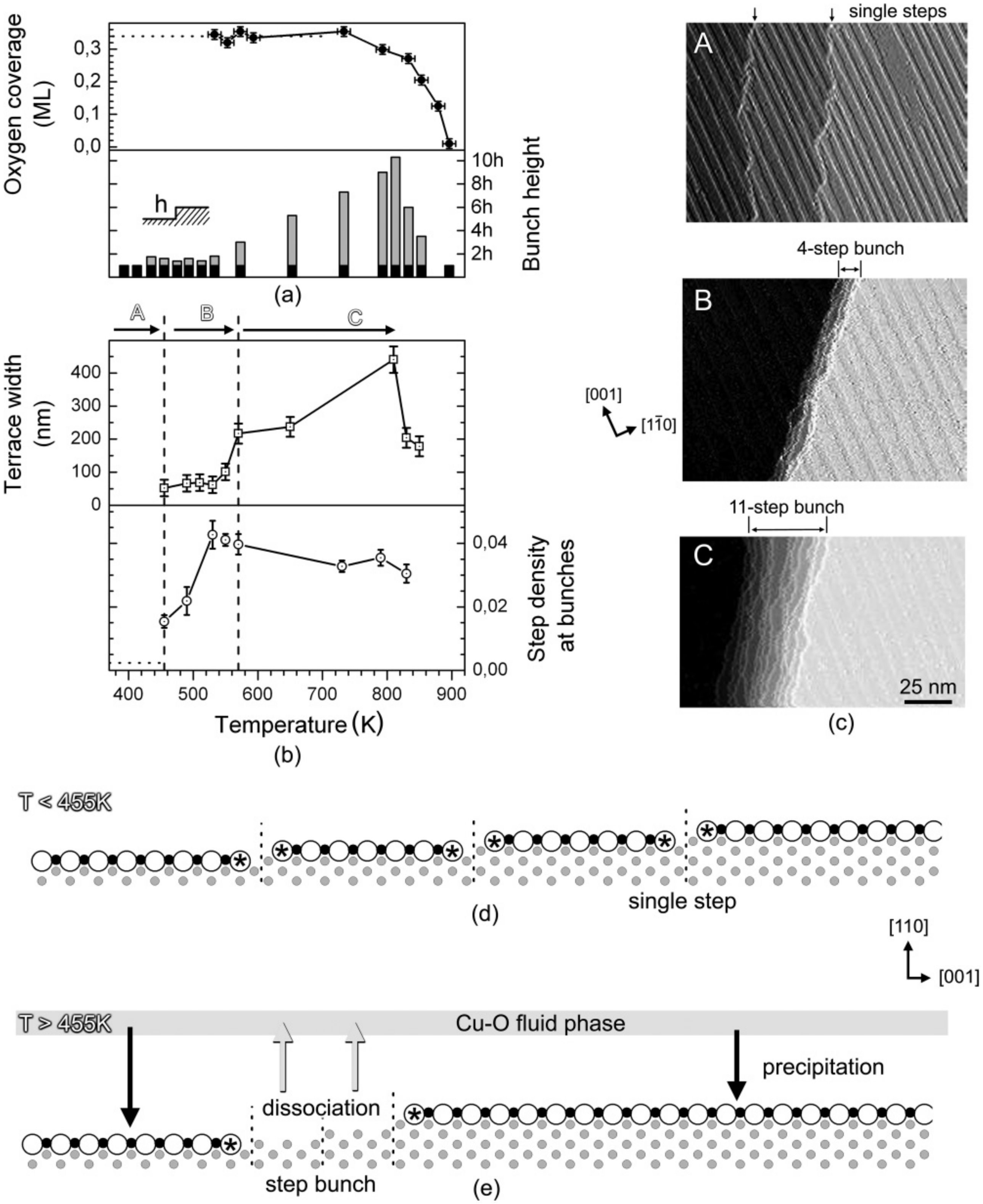

FIG. 7. Step bunching as a function of annealing temperature. (a) Top panel: Oxygen coverage as a function of annealing temperature (black circles). The dotted line depicts the initial oxygen coverage. Bottom panel: The averaged height of the step bunches as a function of annealing temperature. The monoatomic step height is highlighted by black. (b) Averaged terrace width (top panel) and step density at bunches (bottom panel) as a function of annealing temperature. The dashed lines depict the temperature range of the three different regimes (A, B, and C) of the surface rearrangement. The dotted line on the bottom panel indicates the density of surface steps on the oxygenated terraces. (c) STM topographies taken on the surface steps and step bunches after thermal annealing at (A) 455, (B) 570, and (C) 810 K. (d), (e) Side view on the Cu(110) surface under the rearrangement. The black and white circles represent oxygen and copper atoms of the (2×1)–O bands located on the flat terraces (gray circles) separated by either surface steps or step bunches (dotted lines). Here [1$\bar{1}$0] boundaries of the (2×1)–O bands are marked by asterisks.

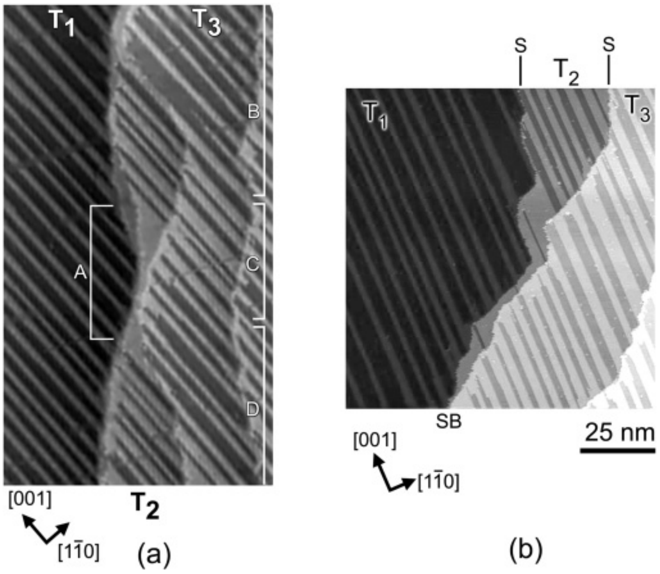

FIG. 8. (a), (b) STM topographies recorded on shrinking terraces of the Cu(110)–(2 × 1)–O surface. The surface terraces (*T*) are marked in ascending order. (a) White brackets (A–D) mark specific zones on corresponding terraces. (b) Surface steps (*S*) and step bunches (SB) are specified.

density (zone C), or the T_3 terrace edge propagates most on the adjacent T_2 terrace by incorporation of Cu atoms at the location with the highest (2 × 1)–O band density (zones B and D). It seems that both processes contribute to the observed terrace width variation. The T_1 terrace reacts with the mobile oxygen in a similar way. The terrace undergoes the most significant etching at the location (zone A), where its own edge was not protected by the (2 × 1)–O bands against the Cu abstraction.

Figure 8(b) shows a later stage of the surface rearrangement, which closely precedes the formation of a step bunch. Following the T_2 terrace in the downward direction on the topography, it can be seen that the terrace underwent significant etching because the scarcely present (2 × 1)–O bands could not prevent the Cu abstraction. Under the oxygen attack, the T_2 terrace is shrinking, losing all its (2 × 1)–O bands and gradually producing a step bunch.

3. Initialization of the surface rearrangement

In this section we will show that interplay between short- and long-range surface interactions induces the inhomogeneous redistribution of the (2 × 1)–O bands between the surface terraces and initiates the surface rearrangement. The elastically driven spatial ordering of the (2 × 1)–O bands on a single terrace has been studied previously by us.[19] Here, we consider global ordering of the (2 × 1)–O bands belonging to different surface terraces.

Figures 10(a)–10(c) represent width distributions of the (2 × 1)–O bands as a function of annealing temperature. The spatial rearrangement of these bands on the Cu(110) surface during annealing is shown schematically in Fig. 10(d). The histograms shown in Figs. 10(a) and 10(b) indicate that the thermal annealing first caused band ripening: The wider bands grow at the expense of the narrower ones [Fig. 10(d), top panel]. The narrow (2 × 1)–O bands, those containing two to six Cu–O chains [Fig. 8(a)], disappear after the 550 K annealing, whereas the number of wider bands (10–14 Cu–O chains) increases [Fig. 10(b)]. This is explained readily by the faster dissociation of the narrow (2 × 1)–O bands under thermal annealing. Consequent precipitation of the Cu–O fluid phase during the cooling down of the surface produces preferentially bigger bands because they are more thermodynamically stable, as discussed in Sec. III B.

The long-range elastic relaxation of the Cu(110)–(2 × 1)–O surface occurs simultaneously with the band ripening and dominates at higher temperatures [Fig. 10(c)]. However, with respect to the band ripening, it operates in the opposite direction. The wider bands visible in Fig. 10(b) become narrower, leading to a more uniform width distribution [Fig. 10(c)]. An important point is that this later transformation does not proceed via the Cu–O fluid phase: The bands relax elastically via surface diffusion of single Cu–O chains [Fig. 10(d)].

So it seems that a dynamical equilibrium exists between ripening and elastic relaxation processes: The uniform (2 × 1)–O bands, albeit being constantly and locally perturbed by the reversible thermal dissociation [Eq. (1)], are prevented from ripening by the elastic relaxation, favoring a uniform band width on the relaxed surface. However, this equilibrium can be reached only within a single terrace.

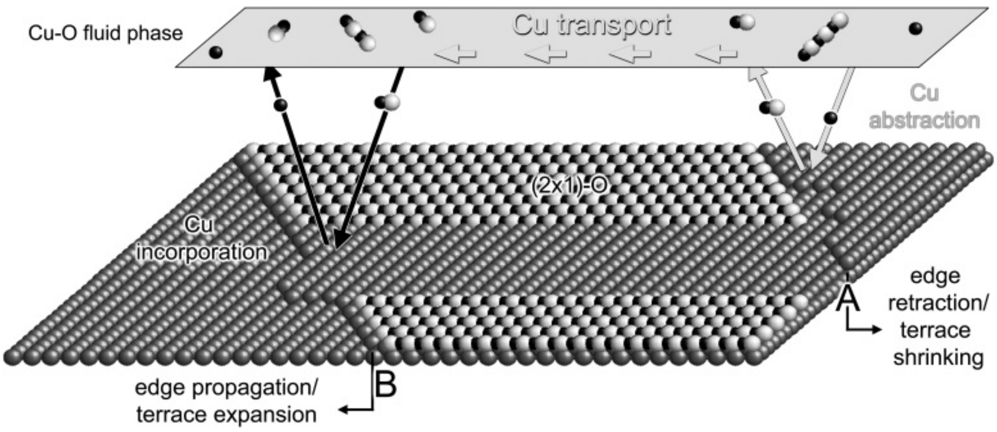

FIG. 9. Mechanism of the thermally induced re-arrangement of the Cu(110)–(2 × 1)–O surface. The gray circles represent the Cu atoms of the substrate. The black and white circles represent O and Cu atoms included into the Cu–O chains or their fragments.

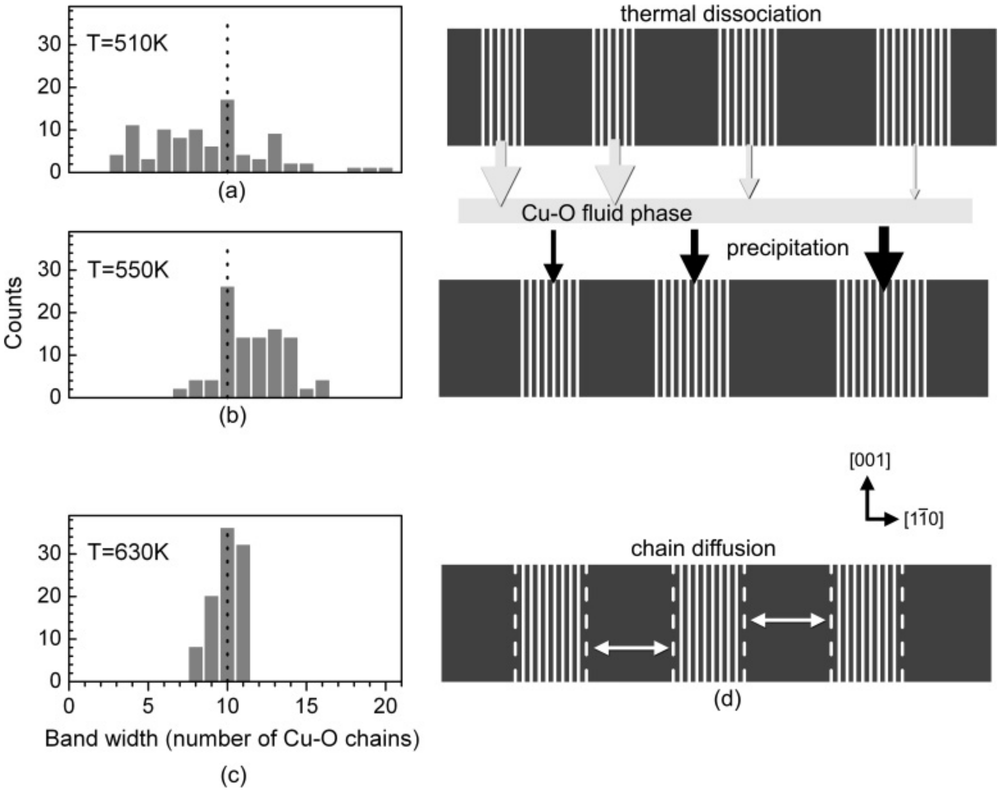

FIG. 10. (a)–(c) Distribution of the (2×1)–O bands in width measured as a function of annealing temperature. (d) Top view on the (2×1)–O bands. The Cu–O chains are shown schematically as white lines on the dark background (Cu substrate). The arrows differing in size reflect the band-specific rate of the dissociation and precipitation processes.

Surface steps and step bunches represent natural obstacles for the Cu–O chain diffusion that prevents establishing a uniform chain distribution between different terraces. The inhomogeneous Cu–O chain distribution on the terrace edges (Fig. 8) made their reactivity site dependent, as it is shown schematically in Fig. 9. This breaks locally the dynamic balance between etching and deposition processes [Eq. (2)] and triggers the selective terrace etching, as we described in Sec. III C 2.

D. Surface rearrangement at high temperatures

With a temperature increase, the reversible dissociation of (2×1)–O chains [Eq. (1)] supplies more Cu–O fragments to the fluid phase. Dissociation of the Cu–O fragments on the terrace edges [Eq. (2)] increases the concentration of mobile oxygen adatoms on the surface. In the 680–740 K range mobile oxygen is capable of overcoming the stabilization barrier, which protected the edges against etching at lower temperatures. This situation is manifested on the topographies shown in Figs. 11(a)–11(c) by formation of the [001] monoatomic height steps (marked by arrows) within the step bunches. At the [001] steps, the chemisorbed oxygen is rearranged into an up to now unknown ×5 reconstructed adsorption phase [Fig. 11(d)]. Its structural model is shown in Figs. 11(d) and 11(e). As in case of oxygen adsorption on the clean surface (Fig. 1), the ×5 phase protects the [001] edges against oxygen attack in the [1$\bar{1}$0] direction. The straight [001] steps propagate laterally on the surface at higher temperature [Fig. 11(c)].

Further thermal annealing results in oxygen desorption. Thermal dissociation of the Cu–O chains creates a sufficiently high concentration of mobile oxygen adatoms that makes effective the recombination channel [Eq. (3)]. Figure 7(a) indicates that oxygen desorbs gradually at $T > 780$ K and completely vanishes at 900 K. The (2×1)–O bands gradually disappear and no longer stabilize the terrace edges. Self-diffusion on the Cu(110) surface[20,21] redistributes gradually the Cu atoms included into the step bunches uniformly between all the surface terraces [Fig. 5(d)]. The entire process is over at ~900 K, when original terrace widths and monoatomic steps only are restored on the surface [Fig. 5(d)].

E. Strain development during the surface rearrangement

In our previous studies we reported that thermal annealing introduces local strain into the oxygen-adsorbed Cu(110)–O surface.[6,13] The strain developed only on mesoscopically corrugated areas of the surface.[6,13] The STM topography, shown in Fig. 12(a), was then intentionally recorded on such a corrugated area. The A_1 and A_2 domains display the recently identified oxygen-adsorption phase observed in Ref. 6. Here, we try to figure out the mechanism of the local strain development favoring these adsorption phases.

A thorough analysis of the STM topography allows unraveling the complex processes of surface rearrangement inducing the deformed surface area. The orientational phase transition appears through formation of the narrow oxygen-free terraces

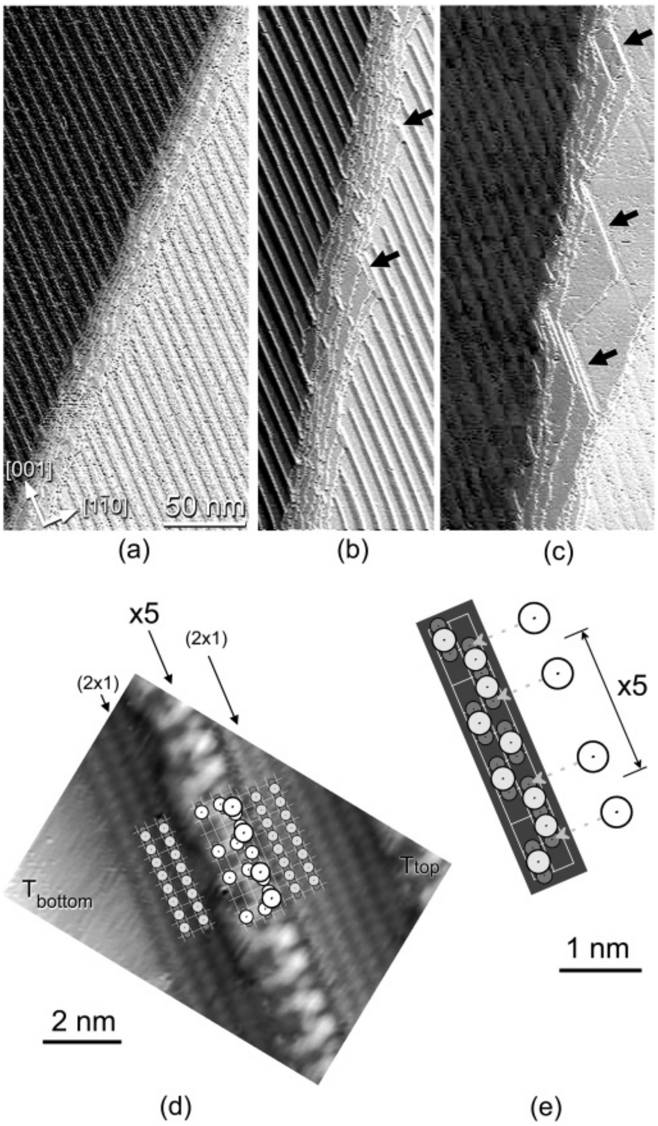

FIG. 11. High-temperature oxygen-induced etching of the step bunches. (a)–(c) STM topographies of a typical step bunch recorded after thermal annealing at (a) 740, (b) 830, and (c) 850 K. (d) STM topography recorded on the [001] monoatomic step between the low-lying (T_{bottom}) and high-lying (T_{top}) terraces. Structural models of the (2×1)–O and $\times 5$ oxygen-adsorption phases [see Fig. 2(c) for notation] are superimposed on the topography. (e) Structural model of the $\times 5$ phase. Four Cu adatoms are shifted aside for clarity; their position in the structure is specified by gray arrows.

(marked by square symbols). They assemble into a step bunch after oxygen-induced etching of the terrace edges. The high-temperature etching of the oxygenated terraces, whose onset was first detected in Figs. 11(a)–11(c), produced surface terrace borders along the [001] direction [marked by cross symbols in Fig. 12(a)]. These terraces are separated by monoatomic steps along [001], which are decorated by the $\times 5$ oxygen-adsorption phase [Fig. 12(b)].

Still, the formation of the T_0 terrace represents a puzzle. None of the processes discussed up to now in this article can explain it. Within the bunch, the T_0 terrace is exceptionally large and it is not bounded by a [001] step. This excludes

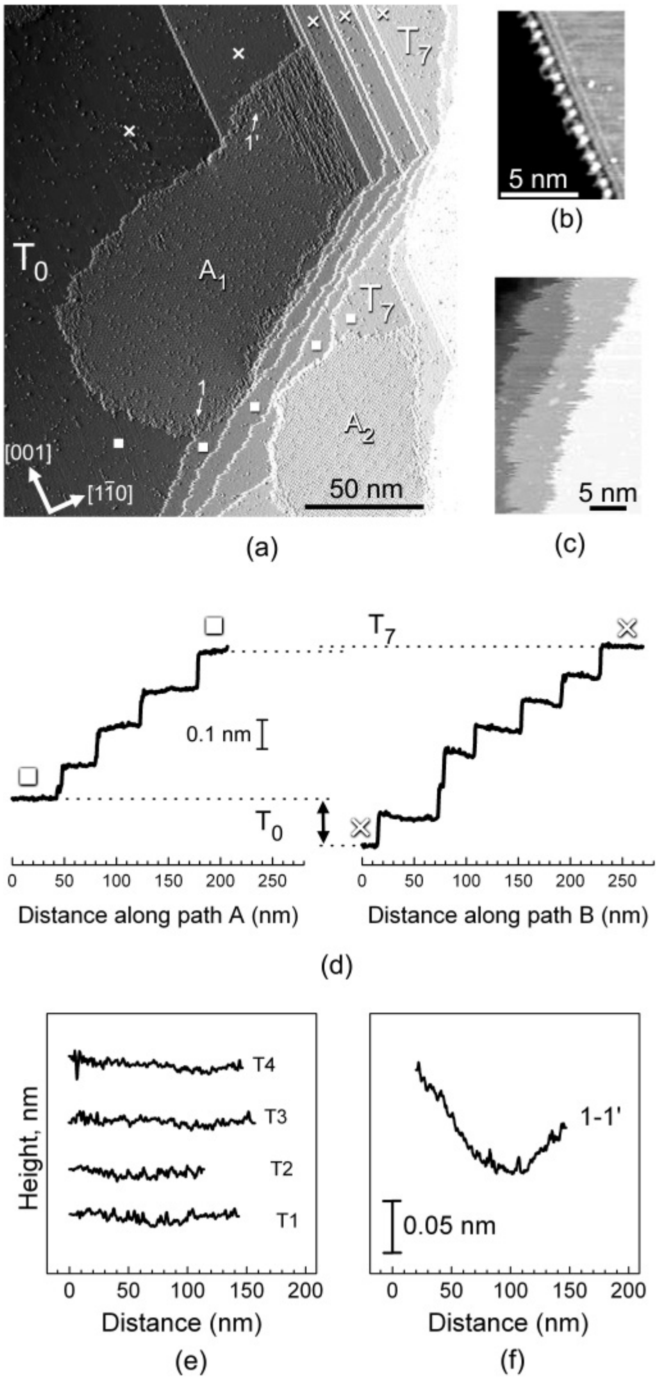

FIG. 12. Strain development during the surface rearrangement. (a) STM topography recorded on a deformed area of the surface. The surface terraces are labeled as $T_0 - T_7$ in ascending order. The square and cross symbols serve as a guide for the eye, designating two paths to ascend from T_0 to T_7 terrace (path A and path B, respectively). The arrows 1 and 1′ depict the lateral position of the height profile shown in (f). (b), (c) STM topographies taken on the [001] steps and terrace edges, respectively. (d) STM height profiles taken along path A (left-hand panel) and path B (right-hand panel) as specified in (a). (e) STM height profiles taken on the $T_1 - T_4$ terraces (marked by squares) along the terrace edges. (f) STM height profile taken on the T_0 terrace as specified in (a).

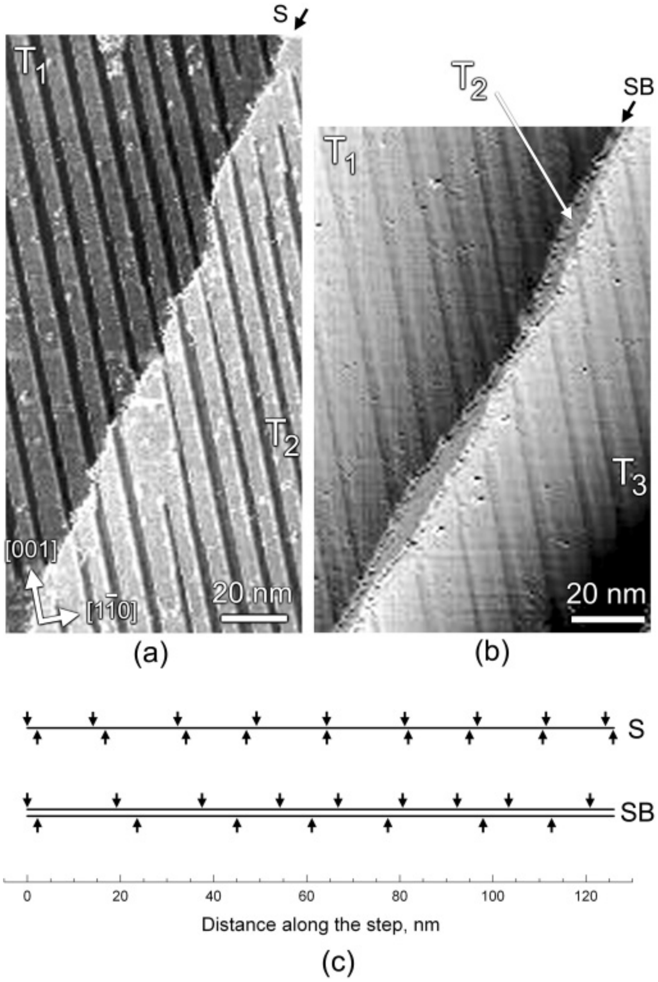

FIG. 13. Longitudinal alignment of the (2 × 1)–O bands. STM topographies of the Cu(110)–(2 × 1)–O surface recorded on (a) a monoatomic step (S) between two adjacent terraces, T_1 and T_2, and (b) a step bunch (SB) produced by the narrow T_2 terrace separating the T_1 and T_3 terraces. (c) Schematics of the (2 × 1)–O bands across the step (S) and the step bunch (SB). The arrows specify the position of the (2 × 1)–O bands.

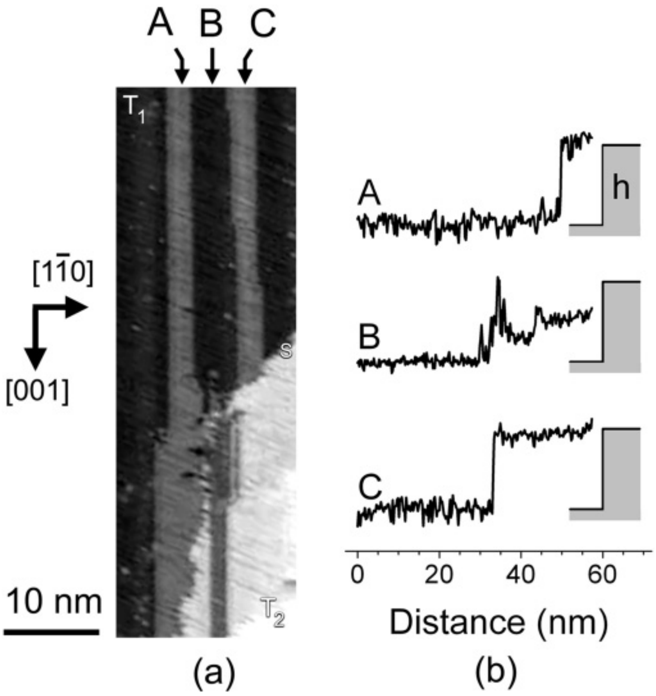

FIG. 14. Fusion of the (2 × 1)–O bands across a monoatomic surface step. (a) The STM topography showing a fusion event between the (2 × 1)–O bands of two adjacent terraces (T_1 and T_2) separated by monoatomic step (S). Arrows mark lateral position of the A, B, and C height profiles shown in (b). (b) The A, B, and C height profiles taken across the monoatomic step along the [001] direction. The height of a monoatomic step (h) is specified for each profile.

the high-temperature etching as a reason for its formation. The STM height profiles shown in Fig. 12(d) shed light on this issue. These profiles are recorded along two paths, each starting at the lowest terrace T_0 and ending at the highest terrace T_7. Path A is via the step bunch, and the corresponding terraces are marked by squares in Fig. 12(a). Path B goes through the [001] steps, and the corresponding terraces are marked by crosses. It can be immediately realized that path B accounts for seven monoatomic steps whereas path A accounts for only four monoatomic steps. It means that several terraces along the paths A and B have merged into a single terrace.

To get more insight in the fusion process, we prepared the Cu(110)–(2 × 1)–O surface by oxygen adsorption [Fig. 13(a)]. Here we purposely avoid the formation of step bunches in order to study the interaction of Cu–O chains across a single step. The striking observation is the alignment of the (2 × 1)–O bands on the low-lying terrace (T_1) with those bands belonging to the high-lying terrace (T_2) across the monoatomic step (S). The following two scenarios can be proposed to explain the band alignment. First, longitudinal short-range attraction between the Cu–O chains can induce their alignment, triggering alignment of the whole bands. Second, the alignment can be induced by elastic relaxation of the surface as a whole.[2–4] In order to discriminate between these two scenarios, we slightly annealed the surface to cause step bunches to appear. The STM topography recorded on one step bunch is shown in Fig. 13(b). Analysis of the STM topographies supports the short-range interaction scenario. Figure 13(c) shows the position of the (2 × 1)–O bands with respect to the S and SB edges (marked by arrows). It can be seen that across the step bunch no alignment occurs: The intermediate T_2 terrace separates spatially the T_1 and T_3 terraces, making impossible the short-range interaction between the corresponding bands. The spatial relaxation of the (2 × 1)–O bands occurs, therefore, independently on each terrace.

The longitudinal alignment of the (2 × 1)–O bands facilitates the terrace fusion. We detected one of such fusion events on the STM topography shown in Fig. 14. Here we captured a moment when two adjacent terraces, T_1 and T_2, are merging. Figure 14(a) shows that the short-range interaction between the two aligned (2 × 1)–O bands (dark strips along B) suppresses the monoatomic step (S) separating the T_1 and T_2 terraces. The A and C height profiles taken along the clean surface areas indicate an ordinal monoatomic step (h) between two terraces. By contrast, no such monoatomic step has been observed on the B profile taken along the (2 × 1)–O bands. The two (2 × 1)–O bands approach each other toward formation of a common band extended on both terraces; their height difference is reduced to be less than the height of the monoatomic step.

Analysis of the individual terraces included into paths A and B allowed us to conclude that, namely, the biggest T_0 terrace contains several terraces merged together. Indeed, the height variation detected on this terrace [0.16 nm as specified by the arrow in Fig. 12(d)] is higher than a monoatomic step height (0.128 nm) and is much higher than the height variation on other terraces (<0.03 nm). The departure point of path B lies 0.16 nm lower (shown by the arrow) than that of path A, whereas both profiles start from the same terrace. It means that the T_0 terrace differs qualitatively from the surrounding terraces; it consists of Cu atoms lying at different heights. The fusion of terraces lying at different heights unavoidably introduces a structural defect into the substrate, followed by substrate deformation and bending of the T_0 terrace. This structural defect is supposed to be a screw dislocation. However, the A_1 adsorbate phase screens the structural defect on the STM topography [Fig. 12(a)] and does not allow one to determine its nature. The height profile taken across the terrace [Fig. 12(f)] shows clearly the curved surface. Other terraces in its vicinity remain flat, and the corresponding height profiles are straight [Fig. 12(e)]. This local substrate deformation initiates strain development, which has been studied in detail in our previous studies.[6,13]

IV. CONCLUSIONS

We have studied the behavior of the oxygen-saturated Cu(110) surface under thermal annealing in the 400–900 K range. We found that the surface is unstable in the whole temperature range owing to a specific interaction of the chemisorbed oxygen with the anisotropic strained surface. The spatially uneven reactivity of the terrace edges with respect to mobile Cu–O fragments induces permanent surface rearrangement into a more thermodynamically stable configuration comprising extremely wide atomically flat [110] terraces fully covered with the well-known (2 × 1)–O bands self-assembled into an ordered superstructure. We anticipate that this feature of the Cu(110)–(2 × 1)–O surface can be very useful in the fabrication of large-scale nanotemplates,[18] guiding the assembly of functional molecules,[14,15] which are of great importance in molecular electronics.[22] In addition, we anticipate that our findings will stimulate fundamental studies aiming at a better understanding of the thermal stability of strained surfaces.

---

[1] D. J. Coulman, J. Wintterlin, R. J. Behm, and G. Ertl, Phys. Rev. Lett. **64**, 1761 (1990).

[2] K. Kern, H. Niehus, A. Schatz, P. Zeppenfeld, J. Goerge, and G. Comsa, Phys. Rev. Lett. **67**, 855 (1991).

[3] Ch. Bombis, M. Moisseva, and H. Ibach, Phys. Rev. B **72**, 245408 (2005).

[4] G. Prevot *et al.*, Surf. Sci. **549**, 52 (2004).

[5] H. Hartman and R. J. Madix, Surf. Sci. **488**, 107 (2001).

[6] K. Bobrov and L. Guillemot, Phys. Rev. B **78**, 121408(R) (2008).

[7] L. Ruan, F. Besenbacher, I. Stensgaard, and E. Laegsgaard, Phys. Rev. Lett. **70**, 4079 (1993).

[8] Y. Kuk, F. M. Chua, P. J. Silverman, and J. A. Meyer, Phys. Rev. B **41**, 12393 (1990).

[9] F. Jensen, F. Besenbacher, E. Laegsgaard, and I. Stensgaard, Phys. Rev. B **42**, 9206 (1990).

[10] L. D. Sun, M. Hohage, R. Denk, and P. Zeppenfeld, Phys. Rev. B **76**, 245412 (2007).

[11] F. Jensen, F. Besenbacher, E. Laegsgaard, and I. Stensgaard, Phys. Rev. B **41**, 10233 (1990).

[12] J. Wintterlin *et al.*, J. Vac. Sci. Technol. B **9**, 902 (1991).

[13] L. Guillemot and K. Bobrov, Phys. Rev. B **79**, 201406(R) (2009).

[14] Y. Naitoh *et al.*, J. Phys. Chem. C **12**, 16118 (2008).

[15] R. Otero *et al.*, Angew. Chem. Int. Ed. **43**, 2092 (2004).

[16] H.-C. Jeong and E. D. Williams, Surf. Sci. Rep. **34**, 171 (1999).

[17] N. Reinecke, S. Reiter, S. Vetter, and E. Taglauer, Appl. Phys. A **75**, 1 (2002).

[18] F. M. Chua, Y. Kuk, and P. J. Silverman, Phys. Rev. Lett. **63**, 386 (1989).

[19] K. Bobrov and L. Guillemot, Surf. Sci. **604**, 1894 (2010).

[20] M. Karimi, T. Tomkowski, G. Vidali, and O. Biham, Phys. Rev. B **52**, 5364 (1995).

[21] H. Yildirim, A. Kara, S. Durukanoglu, and T. S. Rahman, Surf. Sci. **600**, 484 (2006).

[22] J. V. Barth, G. Constantini, and K. Kern, Nature (London) **437**, 671 (2005).